LASER
& PHOTONICS
REVIEWS

Supporting Information

for *Laser Photonics Rev.*, DOI 10.1002/lpor.202300729

An RGB-Achromatic Aplanatic Metalens

Junhao Li, Wenwei Liu, Haofei Xu, Zhaorui Huang, Jian Wang, Jing Wen, Jia Yang, Jianguo Guan, Shuming Wang, Andrea Alù, Zhang-Kai Zhou, Shuqi Chen* and Lin Chen**

Supporting Information

An RGB-achromatic aplanatic metalens

Junhao Li[1,†], *Wenwei Liu*[2,†], *Haofei Xu*[3,†], *Zhaorui Huang*[1], *Jian Wang*[1], *Jing Wen*[4], *Jia Yang*[5], *Jianguo Guan*[6], *Shuming Wang*[7], *Andrea Alù*[8,9], *Zhang-Kai Zhou*[3,*], *Shuqi Chen*[2,*], *and Lin Chen*[1,*]

[1]Wuhan National Laboratory for Optoelectronics and School of Optical and Electronic Information, Huazhong University of Science and Technology, Wuhan 430074, China

[2]The MOE Key Laboratory of Weak Light Nonlinear Photonics, School of Physics and TEDA Institute of Applied Physics, Nankai University, Tianjin 300071, China

[3]State Key Laboratory of Optoelectronic Materials and Technologies, School of Physics, Sun Yat-sen University, Guangzhou 510275, China

[4]Engineering Research Center of Optical Instrument and Systems, Ministry of Education and Shanghai Key Lab of Modern Optical System, University of Shanghai for Science and Technology, Shanghai 200093, China

[5]R&D Department, China Academy of Launch Vehicle Technology, Beijing 100076, China.

[6]State Key Laboratory of Advanced Technology for Materials Synthesis and Processing, Wuhan University of Technology, Wuhan 430074, China

[7]National Laboratory of Solid State Microstructures, School of Physics, Nanjing University, Nanjing 210093, China

[8]Photonics Initiative, Advanced Science Research Center, City University of New York, New York, NY 10031, USA

[9]Physics Program, Graduate Center, City University of New York, New York, NY 10016, USA

[†]These authors contributed equally to this work.

[*] Email: zhouzhk@mail.sysu.edu.cn, schen@nankai.edu.cn, chen.lin@mail.hust.edu.cn.

Contents

Supplementary Note 1: Phase and amplitude distributions

Supplementary Note 2: Analysis of imaging performance with Fresnel diffraction

Supplementary Note 3: Numerical simulations for the metalenses

Supplementary Note 4: Sample fabrication and measurement setup

Supplementary Note 5: Microscopic imaging of the metalenses

Supplementary Note 1: Phase and amplitude distributions

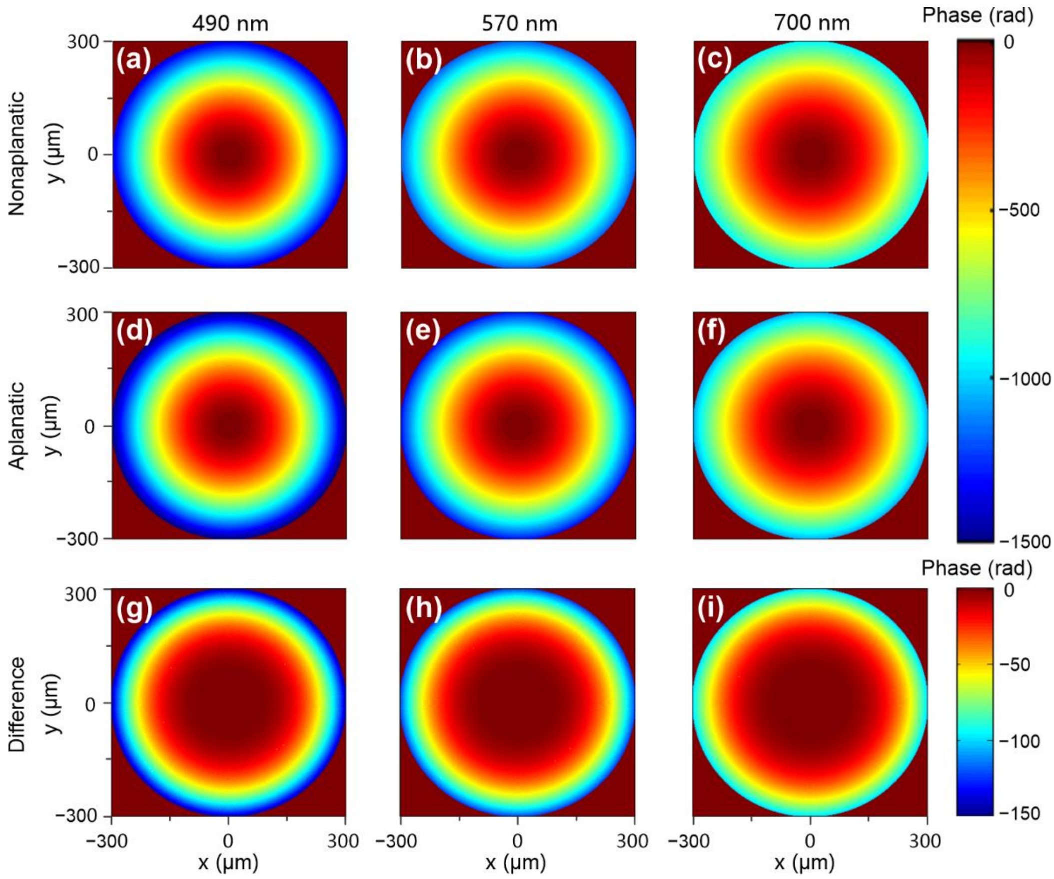

Figure S1. Theoretical phase distributions. (a-c) Phase distributions of the nonaplanatic metalens at 490 (a), 570 (b), and 700 nm (c), respectively. (d-f) Phase distributions of the aplanatic metalens at 490 (d), 570 (e), and 700 nm (f), respectively. (g-i) Distributions of phase difference between the nonaplanatic and aplanatic metalenses at 490 (g), 570 (h), and 700 nm (i), respectively. The nonaplanatic and aplanatic metalenses are with the same focal length of 365 μm and the same NA of 0.635. Considering the fabrication feasibility, the diameter of the circles (or their compensation) is within the range of 100-350 nm. The outer and inner diameters of the rings (or their compensation) are within the range of 200-350 nm and 100-250 nm, respectively, and the difference between the inner and outer diameters is kept larger than 100 nm.

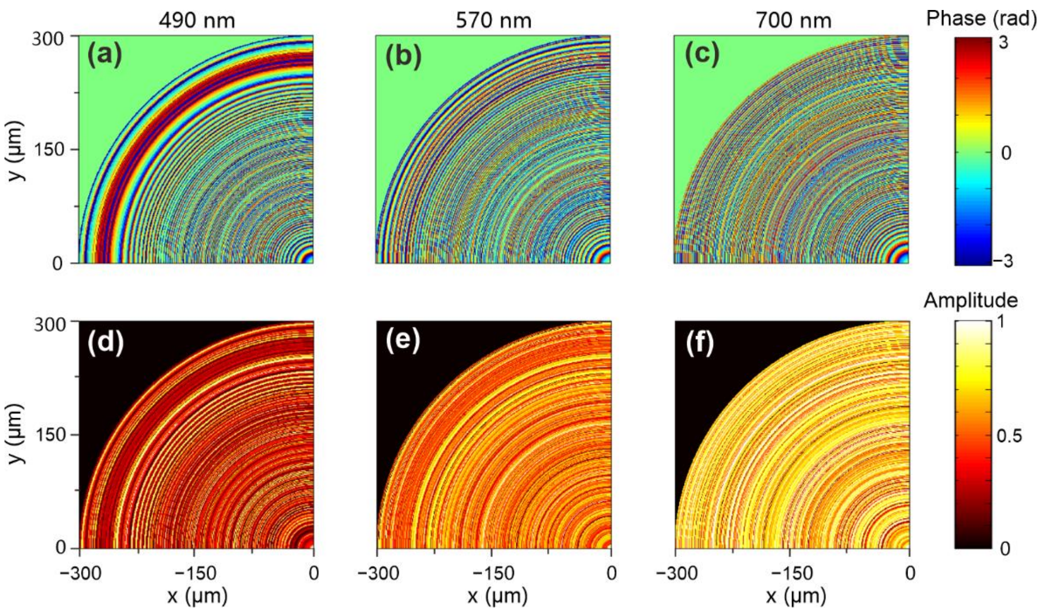

Figure S2. Phase and amplitude distributions realized by the metasurface units. (a-c) Phase distributions of the RGB-achromatic aplanatic metalens at 490 (a), 570 (b), and 700 nm (c). (d-f) Amplitude distributions of the RGB-achromatic aplanatic metalens at 490 (d), 570 (e), and 700 nm (f). The RGB-achromatic aplanatic metalens is with a focal length of 365 μm and an NA of 0.635.

Supplementary Note 2: Analysis of imaging performance with Fresnel diffraction

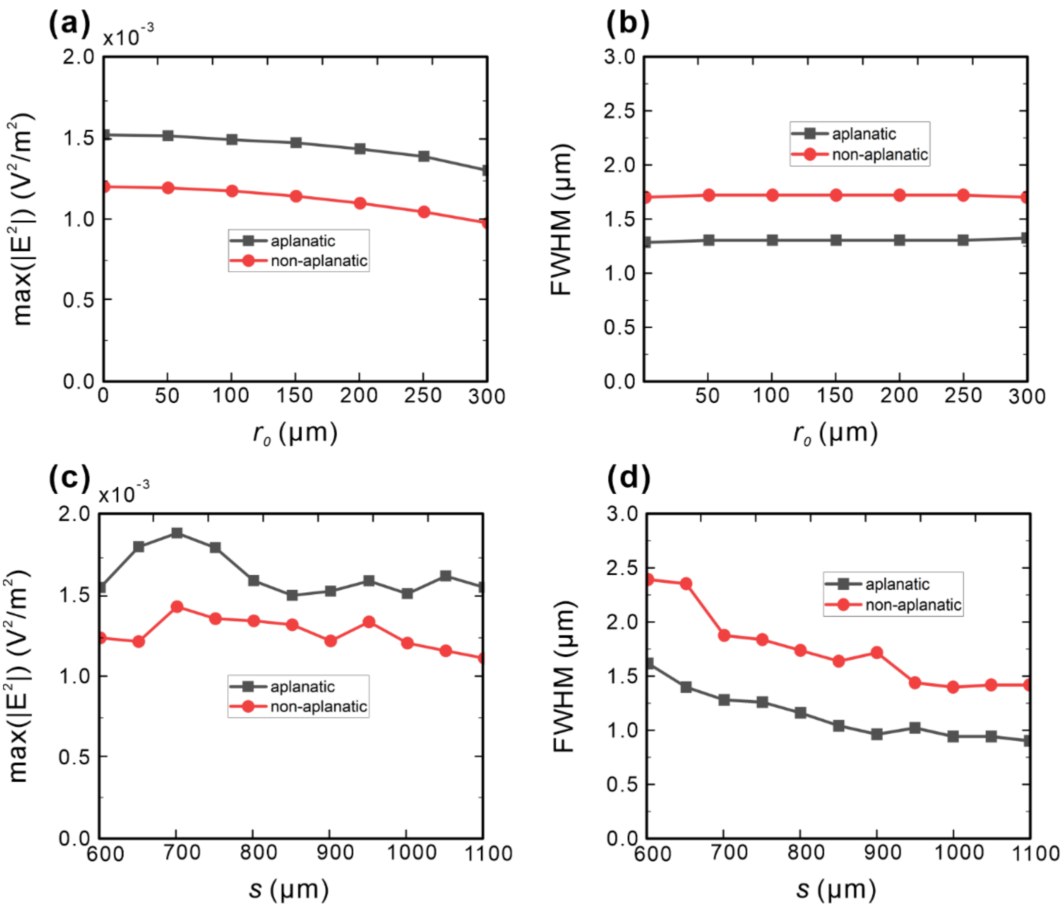

Figure S3. Simulation results with Fresnel diffraction. (a-b) The maximum $|E^2|$ on the imaging plane [$\max(|E^2|)$] and full width at half-maximum (FWHM) as a function of the lateral distance of the object point to the optical axis, r_o, for the RGB-achromatic aplanatic (a) and nonaplanatic (b) metalenses. The object distance is fixed at $s = 700\ \mu\text{m}$. (c-d) $\max(|E^2|)$ and FWHM as a function of object distance, s. The phase profiles of the RGB-achromatic aplanatic and nonaplanatic metalens are the same as that in Fig. 1b, e. In the simulation, the object is set as a 200 nm × 200 nm square with uniform electric field amplitude of 1 V/m. The SiO_2 substrate is with a thickness of $t_s = 400\ \mu\text{m}$, and the incident wavelength is 570 nm.

Supplementary Note 3: Numerical simulations for the metalenses

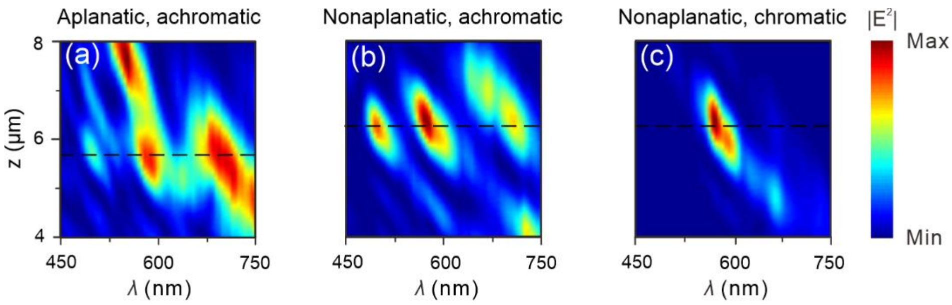

Figure S4. Simulated focusing results of the metalenses. (a-c) Contour plots of normalized $\left|E^2\right|$ versus λ and z under x-polarized normal incidence for an RGB-achromatic aplanatic metalens (a), an RGB-achromatic nonaplanatic metalens (b), and a chromatic nonaplanatic metalens (c). All these metalenses are with $s = 10\ \mu\text{m}$, $s' = 30\ \mu\text{m}$, $t_s = 5\ \mu\text{m}$, and a diameter of 20.4 μm.

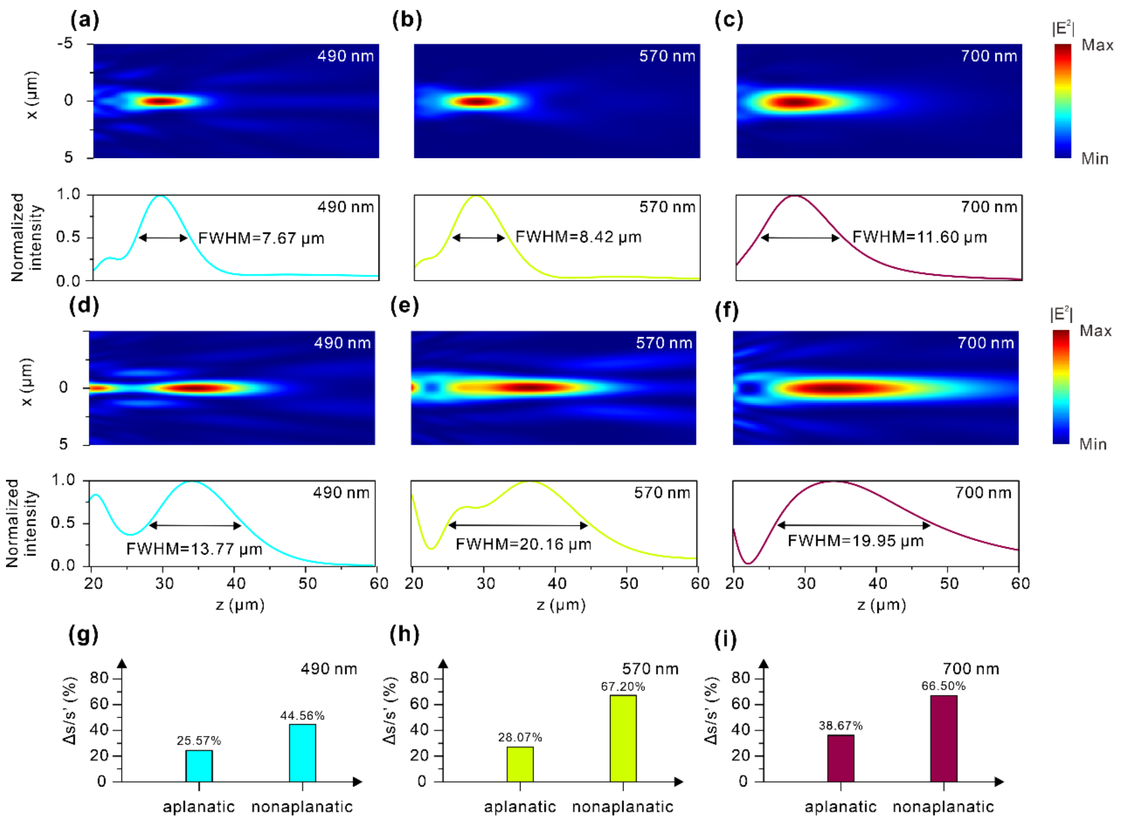

Figure S5. The imaging results of the metalenses illuminated by a point source from FDTD simulation. (a-f) Normalized $|E^2|$ distributions in the x-z plane and field intensity profiles along the z-axis for an RGB-achromatic aplanatic metalens (a-c), and for an RGB-achromatic nonaplanatic metalens (d-f). (g-i) Comparison of the spherical aberration ($\Delta s / s'$) between an RGB-achromatic aplanatic and nonaplanatic metalens at 490 nm (g), 570 nm (h), and 700 nm (i). The geometrical parameters, and object and imaging distances are all the same as those used in Figure S4.

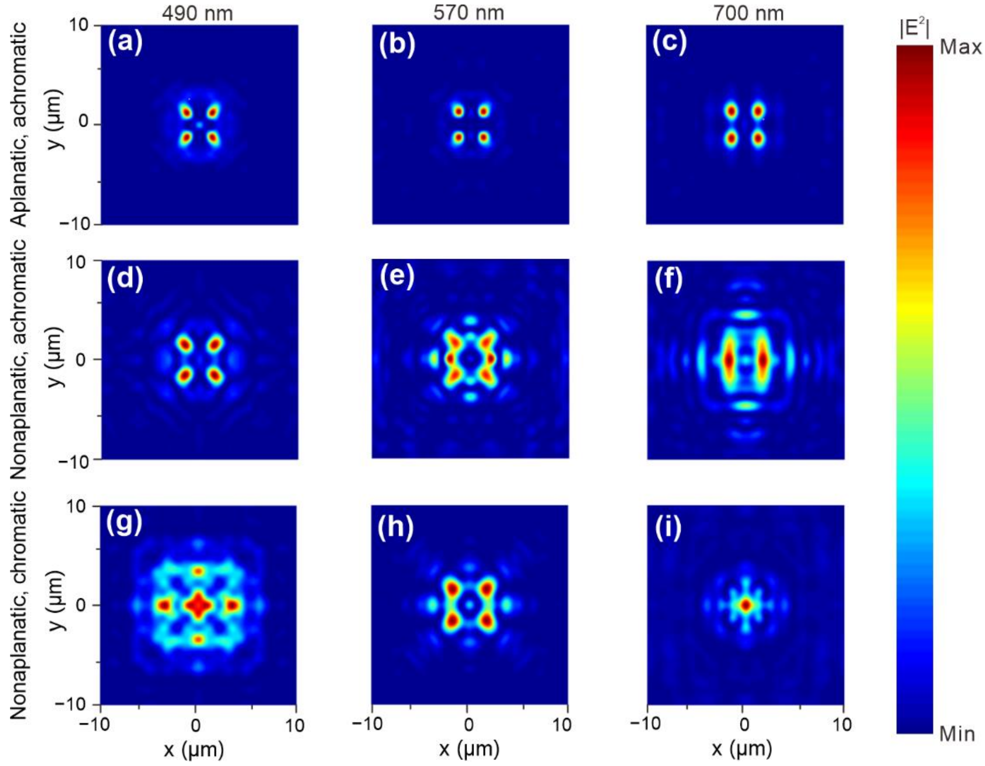

Figure S6. Simulated imaging results of the metalenses. Normalized $\left|E^2\right|$ distributions in the image plane for an RGB-achromatic aplanatic metalens (a-c), an RGB-achromatic nonaplanatic metalens (d-f), and a chromatic nonaplanatic metalens (g-i). The light source is composed of four point-sources on the vertices of a 1 μm × 1 μm square centered on the optical axis. All these metalenses are with $s = 10$ μm, $s' = 30$ μm, $t_s = 5$ μm, and a diameter of 20.4 μm.

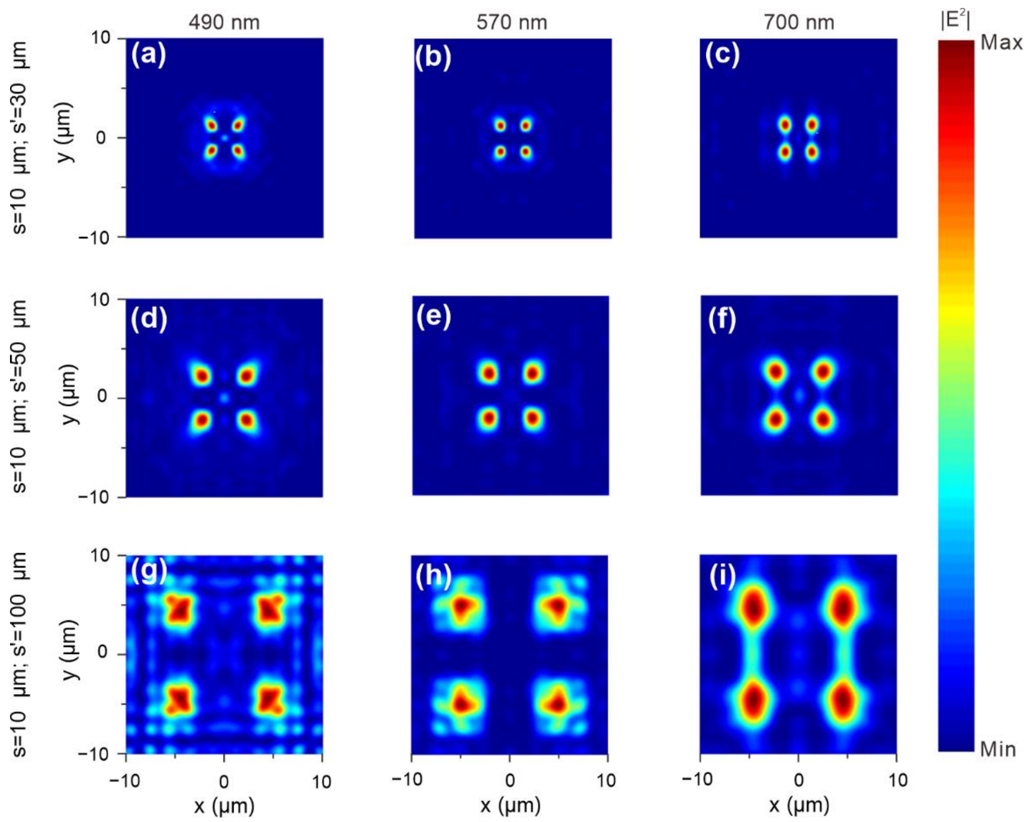

Figure S7. Simulated imaging results of RGB-achromatic aplanatic metalens with different magnifications. Normalized $\left|E^2\right|$ distributions in the image plane for an RGB-achromatic aplanatic metalens with $s = 10$ μm and $s' = 30$ μm (a-c), $s = 10$ μm and $s' = 50$ μm (d-f), and $s = 10$ μm and $s' = 100$ μm (g-i). The light source is composed of four point-sources on the vertices of a 1 μm × 1 μm square centered on the optical axis. All these metalenses are with $t_s = 5$ μm and a diameter of 20.4 μm.

Supplementary Note 4: Sample fabrication and measurement setup

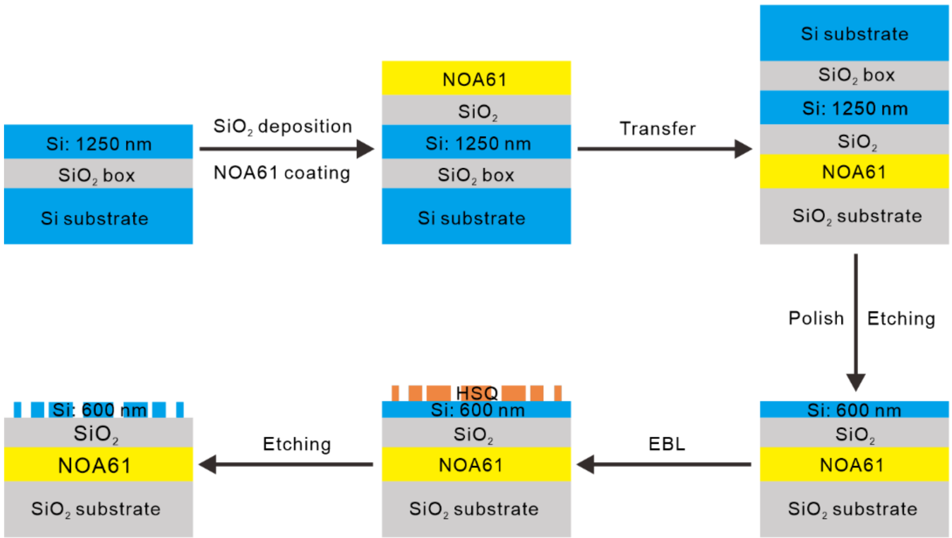

Figure S8. Sample fabrication process. A silica film is deposited on an SOI wafer using inductively coupled plasma chemical vapor deposition (ICP-CVD), followed by spin-coating of the adhesive NOA61. Then, the SOI wafer with silica and NOA61, is bonded with a fused SiO_2 substrate. After exposing with UV light for 4 hours and baking at 50 °C for 3 days, the silicon substrate is removed with polishing and deep reactive ion etching (DRIE), the SiO_2 box layer is removed with HF acid, and the c-Si layer is reduced to 600 nm with ICP. Finally, EBL process and ICP etching are used to obtain the patterned c-Si metasurface.

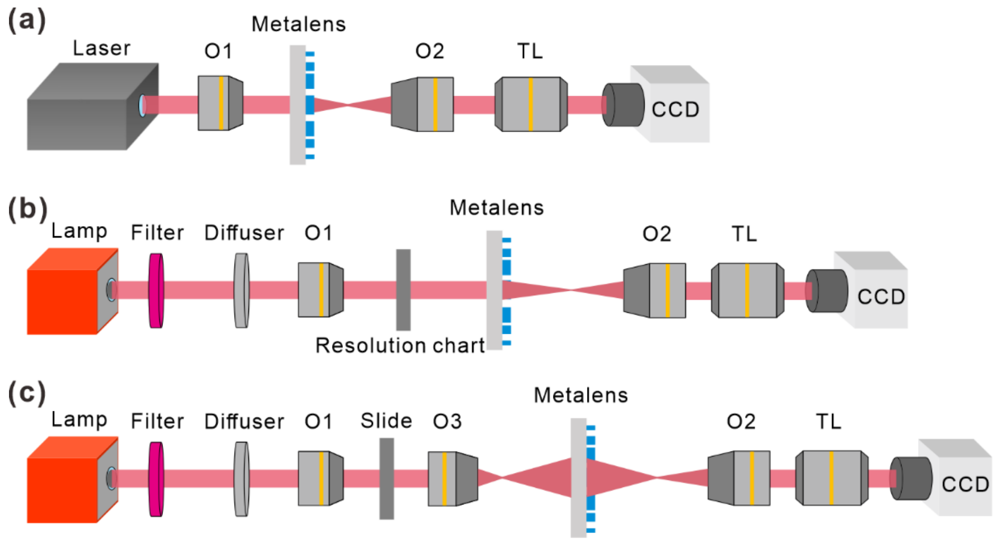

Figure S9. Measurement setup. (a) Measurement setup for focusing. The light from a tunable laser (NKT-SuperK EXTREME) is collected by O1 (objective 1, Sigmakoki EPL-5, 5×, NA = 0.13) and focused by the metalens. The light field is photographed by O2 (objective 2, Sigmakoki EPLE-50, 50×, NA = 0.55), TL (tube lens, Thorlabs, ITL200), and the CCD camera (Hamamatsu, C13440-20CU), all of which are mounted on the same displacement platform to scan different planes. (b) Measurement setup for resolution evaluation. Wide-spectrum white light from a lamp (Thorlabs, SLS401) is filtered by a band-pass filter (Shenzhen NMOT, BP490/BP570/BP700, centered at 490, 570, and 700 nm, respectively, bandwidth of ~20 nm) to characterize the monochromatic imaging performance. The incident light passes through a diffuser to reduce the speckles, and is then collected by O1 to illuminate the resolution chart (the negative 1951 United States Air Force resolution test chart). The image of the metalens is finally photographed by O2, TL, and the CCD camera (monochromatic imaging: Hamamatsu, C13440-20CU). (c) Measurement setup for imaging. The incident light passes through a diffuser to reduce the speckles, and is then collected by O1 to illuminate the slide. For the measurement of color imaging, the filter is removed. The slide for monochromatic imaging is a bee made of a thin Cr film with the laser direct writing method, and the slide for color imaging is fabricated with color printing on highly transparent plastic boards. The image of the slide is zoomed by O3 (objective 3, Sigmakoki EPL-10, 10×, NA = 0.3) to work as the object, which is further imaged by the metalens. The image of the metalens is finally photographed by O2, TL, and the CCD camera (monochromatic imaging: Hamamatsu, C13440-20CU; color imaging: Thorlabs, DCU224C).

Supplementary Note 5: Microscopic imaging of the metalenses

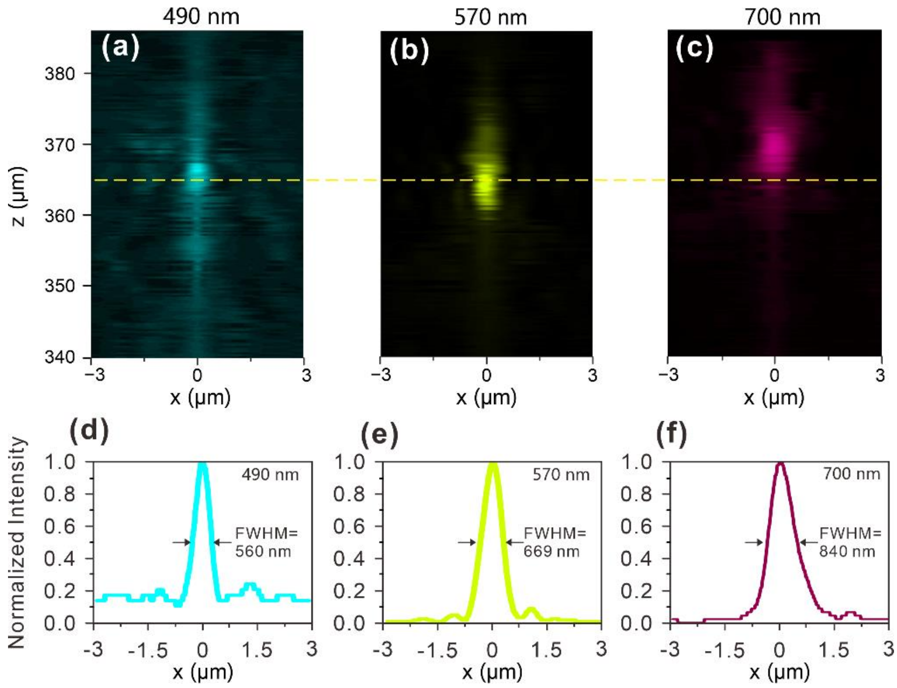

Figure S10. Measured focusing performance of the RGB-achromatic nonaplanatic metalens. (a-c) Light intensity distributions in the x-z plane under a normal incidence at 490 (a), 570 (b), and 700 nm (c). (d-f) The corresponding field intensity profiles along the yellow dashed lines in (a-c).

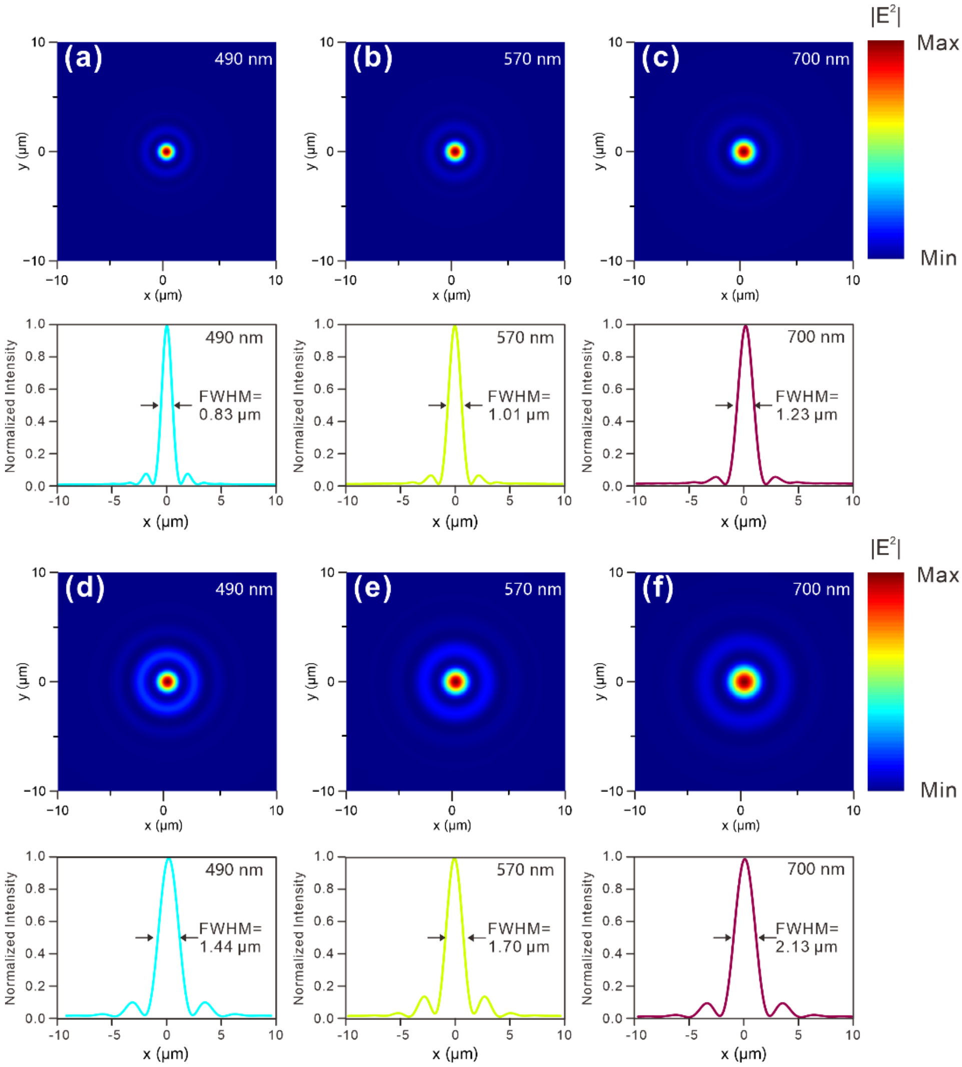

Figure S11. Simulation results with Fresnel diffraction under the illumination of a point source. (a-c) Normalized $|E^2|$ distributions in the image plane and field intensity profiles along the focusing spots at 490 nm (a), 570 nm (b), and 700 nm (c) for the RGB-achromatic aplanatic metalens. (d-f) Normalized $|E^2|$ distributions in the image plane and intensity profiles along the focusing spots at 490 nm (d), 570 nm (e), and 700 nm (f) for the RGB-achromatic nonaplanatic metalens. In the simulation, the object is assumed to be a 200 nm × 200 nm square and has a distance of $s = 700$ μm from the metalenses. The electric field amplitude for the object is assumed to be 1 V/m.

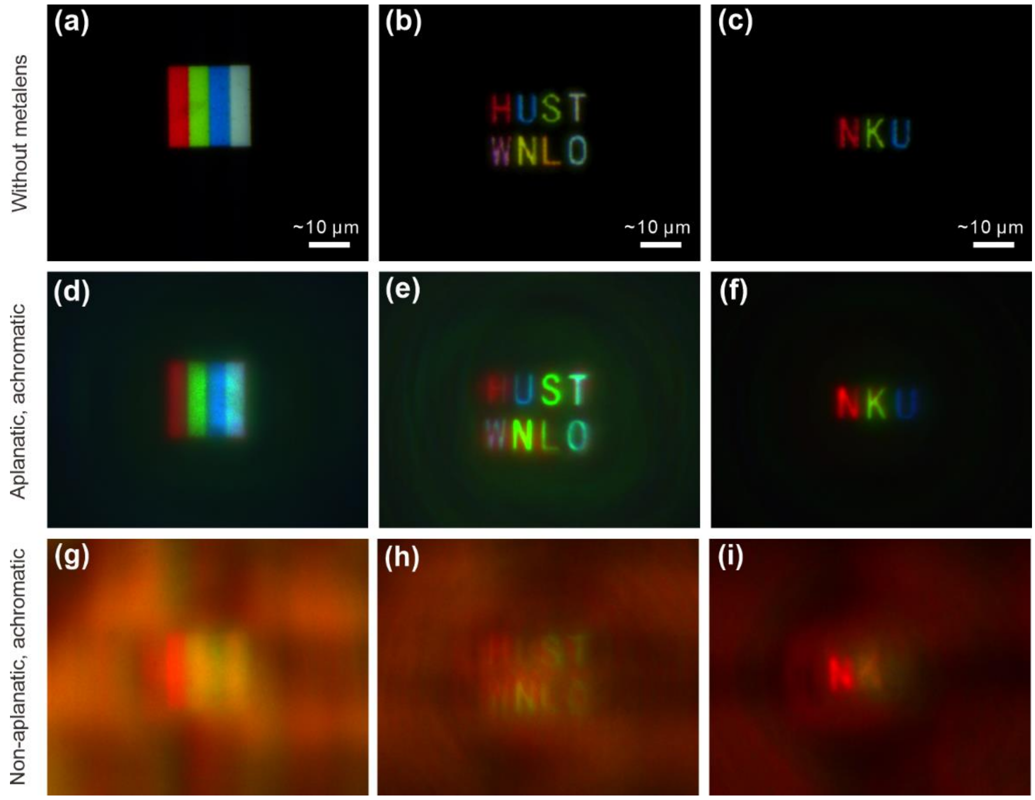

Figure S12. Color imaging performance. (a-c) Images of the color slides without metalens. (d-f) Color images with the aplanatic and achromatic metalens, which are measured with the setup in Figure S9(c) (without the filter).

Supplementary Table S1. Performance comparison.

Reference	NA	Aplanatic	Achromatic	Experimental verification	Compact component	Wave-band
[A1]	0.8	✗	✗	✓	✓	VIS
[A2], [A3]	0.1-0.85	✗	✓	✓	✓	NIR
[A4], [A5], [A6]	0.02-0.2	✗	✓	✓	✓	VIS
[A7]	0.7	✗	✓	✓	✓	VIS
[A8]	0.42	✗	✓	✓	✓	NIR
[A9]	0.04	✗	✓	✓	✗	NIR
[A10]	0.5	✓	✗	✗	✓	VIS
[A11], [A12]	0.8	✗	✓	✓	✓	VIS
[A13]	0.78	✓	✗	✓	✓	VIS
[A14]	1.45	✓	✓	✗	✗	VIS
[A15]	0.7	✗	✓	✓	✓	VIS
Our work	**0.635**	✓	✓	✓	✓	**VIS**

References

[A1] M. Khorasaninejad, W. T. Chen, R. C. Devlin, J. Oh, A. Y. Zhuand F. Capasso, *Science* **2016,** *352*, 1190.

[A2] S. M. Wang, P. C. Wu, V. C. Su, Y. C. Lai, C. H. Chu, J. W. Chen, S. H. Lu, J. Chen, B. B. Xu, C. H. Kuan, T. Li, S. N. Zhuand D. P. Tsai, *Nat. Commun.* **2017,** *8*, 187.

[A3] S. Shrestha, A. C. Overvig, M. Lu, A. Steinand N. F. Yu, *Light Sci. Appl.* **2018,** *7*, 85.

[A4] S. M. Wang, P. C. Wu, V. C. Su, Y. C. Lai, M. K. Chen, H. Y. Kuo, B. H. Chen, Y. H. Chen, T. T. Huang, J. H. Wang, R. M. Lin, C. H. Kuan, T. Li, Z. L. Wang, S. N. Zhuand D. P. Tsai, *Nat. Nanotechnol.* **2018,** *13*, 227.

[A5] W. T. Chen, A. Y. Zhu, V. Sanjeev, M. Khorasaninejad, Z. J. Shi, E. Leeand F. Capasso, *Nat. Nanotechnol.* **2018,** *13*, 220.

[A6] W. T. Chen, A. Y. Zhu, J. Sisler, Z. Bharwaniand F. Capasso, *Nat. Commun.* **2019,** *10*, 355.

[A7] Z. Y. Li, P. Lin, Y. W. Huang, J. S. Park, W. T. Chen, Z. J. Shi, C. W. Qiu, J. X. Chengand F. Capasso, *Sci. Adv.* **2021,** *7*, eabe4458.

[A8] Y. Zhou, I. I. Kravchenko, H. Wang, J. R. Nolen, G. Guand J. Valentine, *Nano Lett.* **2018,** *18*, 7529.

[A9] F. Aieta, M. A. Kats, P. Genevetand F. Capasso, *Science* **2015,** *347*, 1342.

[A10] F. Aieta, P. Genevet, M. Katsand F. Capasso, *Opt. Express* **2013,** *21*, 31530.

[A11] Z. J. Shi, M. Khorasaninejad, Y. W. Huang, C. Roques-Carmes, A. Y. Zhu, W. T. Chen, V. Sanjeev, Z. W. Ding, M. Tamagnone, K. Chaudhary, R. C. Devlin, C. W.

Qiuand F. Capasso, *Nano Lett.* **2018,** *18*, 2420.

[A12] W. B. Feng, J. C. Zhang, Q. F. Wu, A. Martins, Q. Sun, Z. H. Liu, Y. Long, E. R. Martins, J. T. Liand H. W. Liang, *Nano Lett.* **2022,** *22*, 3969.

[A13] C. Chen, W. E. Song, J. W. Chen, J. H. Wang, Y. H. Chen, B. B. Xu, M. K. Chen, H. M. Li, B. Fang, J. Chen, H. Y. Kuo, S. M. Wang, D. P. Tsai, S. N. Zhuand T. Li, *Light Sci. Appl.* **2019,** *8*, 99.

[A14] W. T. Chen, A. Y. Zhu, J. Sisler, Y. W. Huang, K. M. A. Yousef, E. Lee, C. W. Qiuand F. Capasso, *Nano Lett.* **2018,** *18*, 7801.

[A15] Z. Y. Li, R. Pestourie, J. S. Park, Y. W. Huang, S. G. Johnsonand F. Capasso, *Nat. Commun.* **2022,** *13*, 2409.